Nonlinear flexoelectricity in noncentrosymmetric crystals

Kanghyun Chu* and Chan-Ho Yang†
Department of Physics, KAIST, Daejeon 305-701, Republic of Korea
(Received 16 February 2017; published 6 September 2017)

We explore the elastic, dielectric, piezoelectric, and flexoelectric phenomenological coefficients as functions of microscopic model parameters such as ionic positions and spring constants in the two-dimensional square-lattice model with rocksalt-type ionic arrangement. Monte Carlo simulation reveals that a difference in the given elastic constants of the diagonal springs, each of which connects the same cations or anions, is responsible for the linear flexoelectric effect in the model. We show the quadratic flexoelectric effect is present only in noncentrosymmetric systems, and it can overwhelm the linear effect in feasibly large strain gradients. It can also be seen that the linear flexoelectric effect is suppressed by increasing the degree of inversion symmetry breaking due to a rigid dipolar feature.

DOI: 10.1103/PhysRevB.96.104102

I. INTRODUCTION

Flexoelectricity, the inducement of an electric polarization by strain gradients, is an electromechanical phenomenon inherent in all dielectric materials in any space group [1–5]. Despite its ubiquity, the study of flexoelectricity has mainly focused on soft materials and liquid crystals [6–8]. The flexoelectric effect in rigid materials was considered insignificant compared to other electromechanical phenomena such as piezoelectricity because a large strain gradient is hard to attain in macroscopic systems without fracturing or cracking. However, the recent advancement of nanoscale technology enables us to manipulate atomic-scale systems such as strain relaxation in misfit strained epitaxial thin films [9–11], domain walls and interfaces [12–14], tip-induced inhomogeneous mechanical deformation [15], and fractures around a crack tip [16]. Observation of a giant strain gradient in the range of 10^5–10^7 m^{-1} is not astonishing any longer in nanoscale research [10,11,17,18].

Currently, the relation between ferroelectricity and strain gradients has become an important topic of research in dielectrics. The flexoelectric coefficients of some oxide materials have been carefully determined by experiments [19–21]. The development of calculation methods and the simulation studies have also provided a deep understanding of flexoelectricity [16,22–26]. Still, the flexoelectric effect under a huge strain gradient, whereby a nonlinear response arises, has been little studied. Considering the crystal symmetry, the second-order flexoelectric effect which is described by seventh- (odd-) order tensor becomes nonzero if the system does not possess an inversion center such as piezoelectric or ferroelectric materials [14,27,28].

Here, we elucidate the microscopic origin of the flexoelectric effect and evaluate the relative strength of the quadratic and linear flexoelectric effects. Starting from the analytic derivation of the electromechanical properties in a one-dimensional ionic chain model, we expand our discussion to the flexoelectricity into two-dimensional systems.

*kanghyunchu@kaist.ac.kr
†chyang@kaist.ac.kr

II. ONE-DIMENSIONAL IONIC CHAIN MODEL

First, we introduce how to extract the intrinsic piezoelectric effect while excluding the surface piezoelectric effect based on a one-dimensional microscopic model in a pedagogical way before beginning a more complex description regarding the strain-gradient effects in a higher dimension. It is also essential in terms of the fact that the analytic form of the piezoelectric polarization is a part of the induced polarization in the case of a strain gradient. Our starting ionic chain model is composed of two parts: point masses (with alternating electric charges $\pm q$) and harmonic massless springs (characterized by elastic constants $k_{1,2}$ or their inverse values, called elastic compliances $s_{1,2}$), as shown in the Fig. 1(a). We assume the alternating positive and negative ions are equally spaced by a distance a at no external perturbations, indicating the lattice parameter is $2a$. The basic mechanical and dielectric responses of the model are given by $\varepsilon = \frac{1}{2a}(s_1 + s_2)T$ and $\Delta p_{\text{u.c.}} = \frac{1}{4}q^2(s_1 + s_2)E$, respectively [29], where ε is strain, T is applied tensional force, $\Delta p_{\text{u.c.}}$ is induced dipole moment per unit cell, and E is external electric field. If we need to break the inversion symmetry, we can take different values of the elastic constants ($k_1 \neq k_2$) and/or choose different interionic spacing. In order to clarify the intrinsic piezoelectric effect, it is convenient to take a dipole-free unit cell as described in Fig. 1(b) because the extrinsic piezoelectricity is reduced to a surface charge effect and its contribution automatically drops from the bulk calculation, as shown in the following equation [30]:

$$p_{\text{u.c.}} = \sum_\alpha q_\alpha X_\alpha(\varepsilon) = \sum_\alpha q_\alpha\left[(1+\varepsilon)X_\alpha^0 + u_\alpha(\varepsilon)\right] = \sum_\alpha q_\alpha u_\alpha(\varepsilon), \tag{1}$$

where $p_{\text{u.c.}}$ is the dipole moment per unit cell and α stands for the ionic index within a unit cell. X_α represents the position of αth ion when the strain ε is applied, while X_α^0 represents the original coordinate, i.e., $X_\alpha(\varepsilon = 0) = X_\alpha^0$. u_α represents the internal strain imposed on the αth ion, and it indicates an additional displacement from the linear scaled position into which an expansion by a factor of $1 + \varepsilon$ transforms X_α^0 [3]. The dipole-free condition guarantees the equality $\sum_\alpha q_\alpha X_\alpha^0 = 0$.

For given T, ε is $\frac{1}{2a}(s_1 + s_2)T$ since the length change of each spring is $s_{1,2}T$. The difference between the internal strains

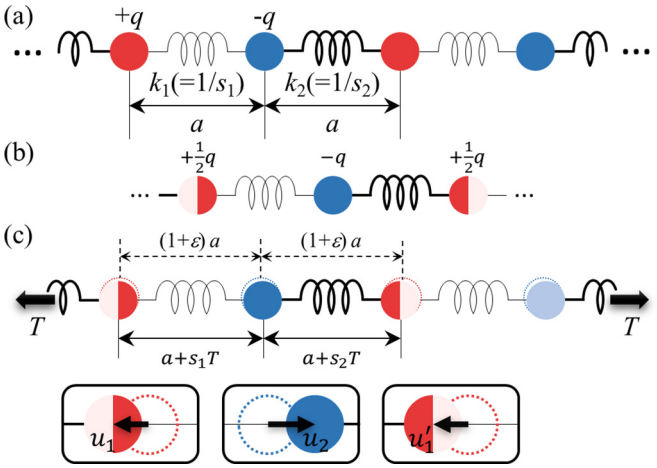

FIG. 1. One-dimensional ionic chain model. (a) The unperturbed state. (b) A dipole-free unit cell. (c) Intrinsic piezoelectric effect. The u_1, u_2, and u_1' are internal strains indicating additional shifts from the linearly scaled-up positions denoted by dashed circles. A situation where the system of $k_2 > k_1$ is under a tensile force is shown.

$u_1 - u_2$ is calculated as $\frac{1}{2}(s_2 - s_1)T$. We note u_1 is equal to u_1' because the discrete translational symmetry is conserved. So the induced piezoelectric dipole moment per unit cell $p_{\text{u.c.}}$ is written as

$$p_{\text{u.c.}} = \frac{q}{2}u_1 - qu_2 + \frac{q}{2}u_1' = q(u_1 - u_2) = \frac{q}{2}(s_2 - s_1)T \left(= qa\frac{s_2 - s_1}{s_1 + s_2}\varepsilon \right). \quad (2)$$

Thus, the piezoelectric coefficient, the dipole moment per unit stress normalized by system size, is $\frac{p_{\text{u.c.}}}{2aT} = \frac{q}{4a}(s_2 - s_1)$. We can identify that the converse piezoelectric coefficient, induced strain per unit electric field, gives the same result, considering a uniform electric field E provokes strain as $\varepsilon(E) = \frac{1}{2a}[\frac{1}{2}(s_2 - s_1)qE]$ [29].

With this in mind, we speculate about the effects on electric polarization by strain gradients in the one-dimension system. For convenience in deriving the flexoelectric coefficient, the unit cell is taken so that it has no electric quadrupole as well as no dipole moment, i.e., satisfying the relations $\sum_\alpha q_\alpha X_\alpha = 0$ and $\sum_\alpha q_\alpha X_\alpha^2 = 0$. Similar to the fact that the dipole-free unit cell is useful in ruling out the extrinsic piezoelectric effect, the virtual unit cell shown in the Fig. 2(a) automatically excludes the surface flexoelectric effect arising from a nonzero quadrupole moment of the system [3]. The unit cell contains partial ions with fractional charges and masses. Although the size of unit cell is larger than the real lattice parameter ($2a$), the repetition of the cells in the interval of $2a$ constructs the original lattice by permission of the overlap. But additional surface charges in finite systems will be necessarily introduced to compensate for the absence of the missing partial charges on the terminations. This is a mathematical trick to nullify the pole moments up to the second-order term, and it has merits in studying bulk properties by explicitly separating them from extrinsic effects.

Provided the system has a homogeneous strain gradient of $\acute{\varepsilon}$, as shown in Fig. 2(b), it is necessarily involved in a

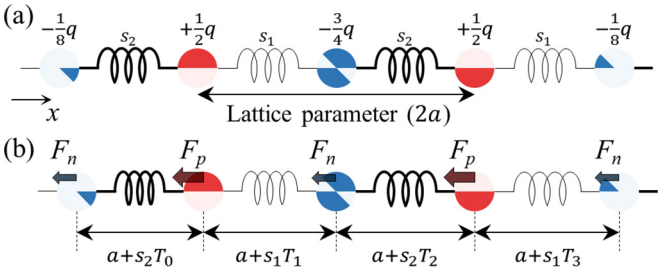

FIG. 2. One-dimensional flexoelectric effect. (a) Dipole- and quadrupole-free unit cell. (b) Strain gradient is driven by external forces acting on cations and anions, which are denoted by F_p and F_n, respectively. For a positive strain gradient of $\frac{\partial\varepsilon}{\partial x}$, $F_p + F_n$ is negative. The intrinsic flexoelectric property is determined by the ratio between F_p and F_n.

tension gradient. They are related to each other by a mechanical coefficient,

$$\frac{\Delta\varepsilon}{\Delta x}(\equiv \acute{\varepsilon}) = \frac{1}{2a}(s_1 + s_2)\frac{\Delta T}{\Delta x}, \quad (3)$$

where x is the spatial coordinate. From a microscopic point of view, the phenomenological strain gradient increases the tension force exerted on the next-nearest-neighbor spring, which has the same elastic constant in the next unit cell, by $2a\frac{\Delta T}{\Delta x}$ compared with that of the original unit cell. However, the phenomenological gradient cannot uniquely determine the relative intra-unit-cell deformations in one-dimensional cases. We have an extra degree of freedom regarding the relative strength of the so-called body forces exerted on positive and negative ions (F_p and F_n). They are responsible for increments between the tension forces of two neighboring springs.

The tension force on each spring, i.e., T_0, T_1, T_2, and T_3 assigned from the leftmost spring, should satisfy the conditions $T_1 = T_0 - F_p$, $T_2 = T_1 - F_n$, and $T_3 = T_2 - F_p$ for the force balance at each ion. The positions of ions are also obtained in a recursive manner as $X_1 = X_0 + a + s_2T_0$, $X_2 = X_1 + a + s_1T_1$, $X_3 = X_2 + a + s_2T_2$, and $X_4 = X_3 + a + s_1T_3$. The induced dipole in the cell is obtained finally as follows:

$$\sum_{\alpha=0}^{4} q_\alpha X_\alpha = \frac{q}{8}(s_1+s_2)(F_p - F_n) + \frac{q}{8}(s_2 - s_1)\left(\sum_{i=0}^{3} T_i\right) = \frac{1}{2}qa^2\frac{F_p - F_n}{F_p + F_n}\acute{\varepsilon} + \frac{q}{2}(s_2 - s_1)\bar{T}. \quad (4)$$

Note that the strain gradient (and the corresponding macroscopic tension gradient) is proportional to $F_p + F_n$. The first term in the last equation is proportional to the given strain gradient $\acute{\varepsilon}$, and thus, the proportional coefficient corresponds to the intrinsic flexoelectric effect. The second term depending on the inversion symmetry breaking $(s_2 - s_1)$ is due to the intrinsic piezoelectric effect, and it has a position dependence as such mean tension of the unit cell $\bar{T}$ does. From the derivation, we can make the conclusion that the dimensionless $\frac{F_p - F_n}{F_p + F_n}(\equiv f)$ is the origin of the linear flexoelectric effect. The term f seems to be arbitrarily chosen in one-dimensional cases, although this ambiguity is removed in higher dimensions, as addressed below. The value can be temporally specified, as a characteristic of the one-dimensional

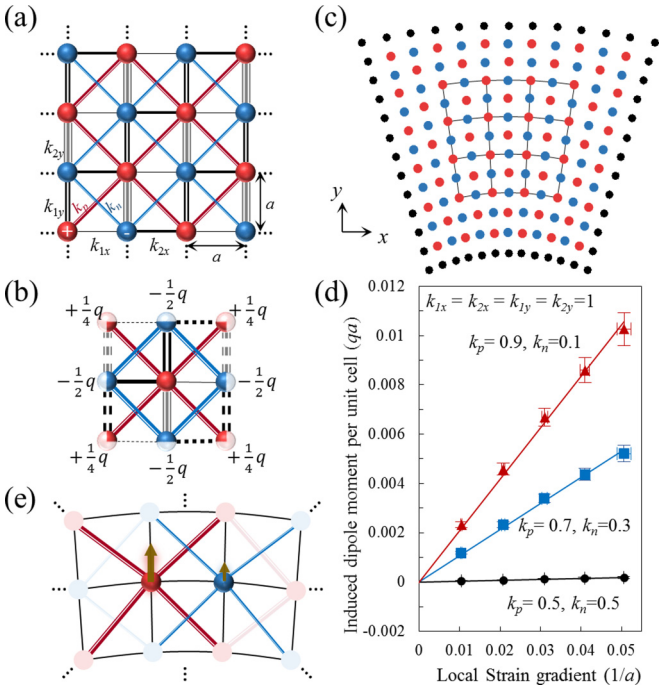

FIG. 3. Two-dimensional ionic chain network model. (a) Model scheme. (b) Pole-free cell. (c) Typical relaxed configuration of the strain gradient of $0.05/a$. Solid black dots are fixed sites. The black guide lines illuminate the 3×3 pole-free cells in use. (d) Induced dipole moment with respect to applied strain gradient. (e) Schematic diagram of linear flexoelectricity.

model, by a sort of bonding property unrelated to the inversion symmetry breaking or conjugate charges of constituent atoms in cases of a uniform external field.

III. SIMULATION STUDY ON TWO-DIMENSIONAL MODEL

A. Linear flexoelectricity

We have performed the simulation study based on a two-dimensional ionic model. It consists of positive and negative ions and elastic springs, as shown in Fig. 3(a). There are six types of springs: two along the x axis (k_{1x}, k_{2x}), another two along the y axis (k_{1y}, k_{2y}), and two connecting ions of the same charges (k_p, k_n) along diagonals. It catches the essence of nearest- and next-nearest-neighbor interactions in a two-dimensional rocksalt structure, which is an easily addressable crystalline system.

We introduce a pole-free double unit cell as displayed in Fig. 3(b). It is convenient to describe the local states based on the cell because the extrinsic piezoelectric and flexoelectric effects are automatically eliminated in the bulk calculation, and all extrinsic effects are converted into the problems related to surface charges and surface dipoles.

The transverse strain gradient $\frac{\partial \varepsilon_{xx}}{\partial y}$ is applied to a model system composed of 5×5 pole-free cells (its size is $2a \times 2a$) as shown in Fig. 3(c). The outermost black dots are fixed sites [29]. Only the 3×3 pole-free cells out of 25 cells are included in the property evaluation to rule out possible clamping effects arising from the constraint edge sites. All the positions of

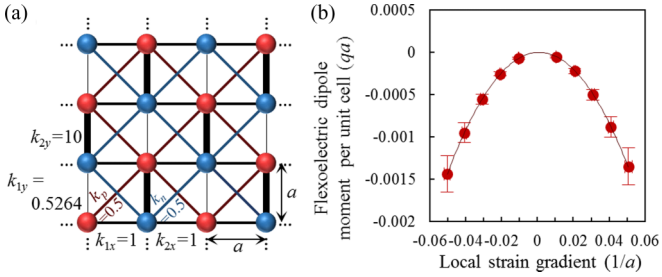

FIG. 4. Quadratic flexoelectric effect in a noncentrosymmetric system. (a) An ionic model with no inversion symmetry as a consequence of the difference in k_{1y} and k_{2y}. (b) Dipole moment per unit cell flexoelectrically induced by the local strain gradient.

ions except for the edge sites are relaxed by the Monte Carlo algorithm until the total elastic energy stored in the springs is minimized.

As a result, the conventional linear flexoelectric effect was numerically reproduced, and it could be manipulated by tuning the diagonal springs. The model systems were designed to be centrosymmetric by setting all springs lying along the x and y axes to be identical to prohibit any intervention of the intrinsic piezoelectric effect. While tuning k_p and k_n, the sum $k_p + k_n$ was kept constant to equalize the elastic property of each model system. Figure 3(d) shows the induced flexoelectric dipole moment as a function of the transverse strain gradient for selected k_p, k_n conditions. Each data point and error bar represent the mean and standard deviation of the local transverse strain gradient and the local y dipole moment obtained from each relaxed configuration containing the nine pole-free cells. A linear relationship between the strain gradient and the induced dipole moment is found, implying conventional linear flexoelectricity.

The lesson from the analytic derivation of the flexoelectric coefficient in the one-dimensional ionic chain is that the linear flexoelectric effect increases as f gets larger. As shown in Fig. 3(e), the transverse strain gradient squeezes the bottom layer, compressing the diagonal springs below, while it expands the top layer, stretching the diagonal springs above. If k_p is larger than k_n, the deformation generates a larger tugging force on the positive ion than that on the negative one. As a consequence, the positive ion shifts upward more than the negative ion, resulting in a positive flexoelectric polarization.

B. Quadratic flexoelectricity

Furthermore, the nonlinear flexoelectric effect arising in noncentrosymmetric systems is simulated. The inversion symmetry is broken along the y axis by discriminating between k_{1y} and k_{2y} [Fig. 4(a)]. A compliance-matching condition $s_{1x} + s_{2x} = s_{1y} + s_{2y}$ is held when modifying the model parameters in order to make the elastic properties along the x and y axes equivalent. In addition, the linear flexoelectric response is eliminated by setting $k_p = k_n$ to focus on the second-order effect. It is worth mentioning that, when $k_{1x} = k_{2x} = k_{1y} = k_{2y}$, the system belongs to the two-dimensional space group *p4mm*; if $k_{1x} = k_{2x}, k_{1y} \neq k_{2y}$, the symmetry is reduced to *cm*. Since the system also has piezoelectricity, separating the piezoelectric contribution from

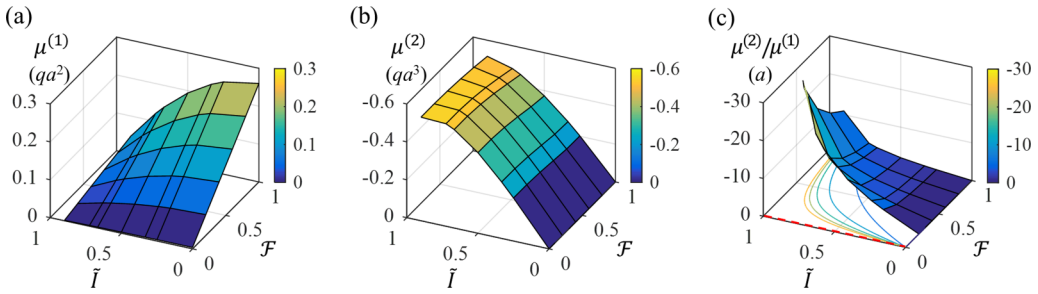

FIG. 5. Flexoelectric coefficient maps. (a) Linear flexoelectric coefficient $\mu^{(1)}$. (b) Quadratic flexoelectric coefficient $\mu^{(2)}$. (c) Ratio of the quadratic coefficient to the linear coefficient. A contour plot for the ratio is also given, and the dashed red line along the $\tilde{I}$ axis represents where the ratio diverges. The parameters $\tilde{I}$ and $\mathcal{F}$ are defined in the main text. The grid intersection points represent the parameters values for which the actual simulation was performed.

the raw simulated data of the induced dipole moment is required to extract the pure flexoelectric effect. We were able to estimate the local piezoelectric dipole moment by using the piezoelectric coefficients and the local strain states [29]. Figure 4(b) exhibits the flexoelectric dipole moment per unit cell obtained by varying the applied strain gradient in the noncentrosymmetric system, indicating the manifestation of a quadratic flexoelectric effect.

Finally, we systematically investigate the flexoelectric coefficients with respect to model parameters. The coefficients $\mu^{(1)}$ and $\mu^{(2)}$ can be determined by fitting the strain-gradient-dependent data to the phenomenological relation:

$$p_{\text{u.c.}}^{\text{flexo}} = \mu^{(1)}\acute{\varepsilon} + \mu^{(2)}\acute{\varepsilon}^2, \tag{5}$$

where $p_{\text{u.c.}}^{\text{flexo}}$ is the induced flexoelectric dipole moment per pole-free cell and $\acute{\varepsilon}$ is the transverse strain gradient. Fixing the spring constants along the x axis ($k_{1x} = k_{2x} = 1$), the spring constants along the y axis and the diagonal axes were varied. At that time, the macroscopic elastic properties of systems were equalized by keeping the constraints $k_p + k_n = 1$ and $s_{1y} + s_{2y} = 2$. Each flexoelectric coefficient is plotted as a function of two dimensionless parameters of $\frac{k_{2y}-k_{1y}}{k_{2y}+k_{1y}} (\equiv \tilde{I})$ and $\frac{k_p-k_n}{k_p+k_n} (\equiv \mathcal{F})$, which are related to the degree of inversion symmetry breaking and the difference in the interaction strengths among the same kind of ions, respectively. As we expect, $\mu^{(1)}$ and $\mu^{(2)}$ turn out to be linearly correlated with $\mathcal{F}$ and $\tilde{I}$, respectively. Interestingly, $\mu^{(1)}$ decreases as the inversion symmetry breaking becomes severe, in addition to the linear dependence on $\mathcal{F}$ [Fig. 5(a)]. It is most likely attributed to the rigid dipolar feature associated with strong k_{2y} and weak k_{1y}. This dimerization hampers ionic redistribution caused by the difference in k_p and k_n under nonzero strain gradients. Meanwhile, $\mu^{(2)}$ is hardly affected by $\mathcal{F}$ [Fig. 5(b)]. The plot of the ratio of the second-order flexoelectric coefficient over the first-order one [Fig. 5(c)] enables the estimation of a threshold strain gradient above which the quadratic flexoelectric effect exceeds the linear effect. Considering the typical atomic distance of a few angstroms, the threshold strain gradient for the parameters along the yellow contour line, for example, is 10^7–10^8 m^{-1}, which is a feasible value reported at the morphotropic phase interfaces where an asymmetric piezoresponse has been found [14]. The quadratic flexoelectric effect is small in most realistic situations. One exception that appears to have been overlooked is fracture physics, which is, by definition, a nonlinear mechanical problem. Crack tips in particular concentrate the largest strain gradients that a material can withstand, and recent calculations show enormous asymmetric flexoelectric polarizations around crack tips [16]. We also note that the corrugated two-dimensional sheets often undergo such large transverse strain gradient. Naumov *et al.* performed a first-principles calculation on a corrugated noncentrosymmetric boron nitride sheet, reporting a nonlinear electromechanical effect [28].

IV. DISCUSSION

Our model system can be extended in various ways. It is possible to consider a more complex unit cell that contains multiple ionic bases and extended neighbor interactions at the expense of rapidly increasing calculation complexity dealing with possible combinations of ions in a unit cell and its neighbors. On the other hand, to handle a system made of a single kind of atoms, it can be treated as a pseudobinary ion system by introducing imaginary ions that stand for the centers of electron clouds [31]. Adopting anharmonic springs allows the model system to represent the effects of electrostriction and second-order piezoelectricity [32–35].

The magnitudes of charges can be considered the formal charges of the ions in a naïve sense. One may also interpret them as the Born effective charges taking electron redistribution into account [36] and the spring constants as the Born–von Kármán force constants [37] beyond the classical picture. On the assumption that the charge is ten times larger than the elementary charge of the electron and a is a few angstroms, the simulated result for the linear flexoelectric coefficient corresponds to $\sim$1 nC/m, which is comparable to the measured quantity in $SrTiO_3$ [21]. Our theoretical approach opens the door to a quantitative understanding of the electromechanical properties in crystals.

ACKNOWLEDGMENTS

This work was supported by the National Research Foundation (NRF) grant funded by the Korean government (Grants No. NRF-2013S1A2A2035418, No. NRF-2014R1A2A2A01005979, No. NRF-2017R1A3B1023686) and the NRF via the Center for Quantum Coherence in Condensed Matter (2016R1A5A1008184) and the Global Frontier R&D Program on Center for Hybrid Interface Materials (2013M3A6B1078872).

[1] S. M. Kogan, Fiz. Tverd. Tela (Leningrad) **5**, 2829 (1963).
[2] A. K. Tagantsev, Sov. Phys. JETP **61**, 1246 (1985).
[3] A. K. Tagantsev, Phys. Rev. B **34**, 5883 (1986).
[4] P. Zubko, G. Catalan, and A. K. Tagantsev, Annu. Rev. Mater. Res. **43**, 387 (2013).
[5] S. Mao and P. K. Purohit, J. Appl. Mech. **81**, 081004 (2014).
[6] R. Meyer, Phys. Rev. Lett. **22**, 918 (1969).
[7] W. Helfrich, Z. Naturforsch. **26a**, 833 (1971).
[8] M. A. Osipov, Sov. Phys. JETP **58**, 1167 (1983).
[9] G. Catalan, B. Noheda, J. McAneney, L. J. Sinnamon, and J. M. Gregg, Phys. Rev. B **72**, 020102 (2005).
[10] D. Lee, A. Yoon, S. Y. Jang, J.-G. Yoon, J.-S. Chung, M. Kim, J. F. Scott, and T. W. Noh, Phys. Rev. Lett. **107**, 057602 (2011).
[11] B. C. Jeon, D. Lee, M. H. Lee, S. M. Yang, S. C. Chae, T. K. Song, S. D. Bu, J.-S. Chung, J.-G. Yoon, and T. W. Noh, Adv. Mater. **25**, 5643 (2013).
[12] G. Catalan, A. Lubk, A. H. G. Vlooswijk, E. Snoeck, C. Magen, A. Janssens, G. Rispens, G. Rijnders, D. H. A. Blank, and B. Noheda, Nat. Mater. **10**, 963 (2011).
[13] A. Y. Borisevich, E. A. Eliseev, A. N. Morozovska, C.-J. Cheng, J.-Y. Lin, Y.-H. Chu, D. Kan, I. Takeuchi, V. Nagarajan, and S. V. Kalinin, Nat. Commun. **3**, 775 (2012).
[14] K. Chu, B.-K. Jang, J. H. Sung, Y. A. Shin, E.-S. Lee, K. Song, J. H. Lee, C.-S. Woo, S. J. Kim, S.-Y. Choi, T. Y. Koo, Y.-H. Kim, S.-H. Oh, M.-H. Jo, and C.-H. Yang, Nat. Nanotechnol. **10**, 972 (2015).
[15] H. Lu, C.-W. Bark, D. Esque de los Ojos, J. Alcala, C. B. Eom, G. Catalan, and A. Gruverman, Science **336**, 59 (2012).
[16] A. Abdollahi, C. Peco, D. Millán, M. Arroyo, G. Catalan, and I. Arias, Phys. Rev. B **92**, 094101 (2015).
[17] T. D. Nguyen, S. Mao, Y.-W. Yeh, P. K. Purohit, and M. C. McAlpine, Adv. Mater. **25**, 946 (2013).
[18] R. J. Zeches, M. D. Rossell, J. X. Zhang, A. J. Hatt, Q. He, C.-H. Yang, A. Kumar, C. H. Wang, A. Melville, C. Adamo, G. Sheng, Y.-H. Chu, J. F. Ihlefeld, R. Erni, C. Ederer, V. Gopalan, L. Q. Chen, D. G. Schlom, N. A. Spaldin, L. W. Martin, and R. Ramesh, Science **326**, 977 (2009).
[19] W. Ma and L. E. Cross, Appl. Phys. Lett. **86**, 072905 (2005).
[20] L. E. Cross, J. Mater. Sci. **41**, 53 (2006).
[21] P. Zubko, G. Catalan, A. Buckley, P. R. L. Welche, and J. F. Scott, Phys. Rev. Lett. **99**, 167601 (2007).
[22] S. V. Kalinin and V. Meunier, Phys. Rev. B **77**, 033403 (2008).
[23] J. Hong and D. Vanderbilt, Phys. Rev. B **84**, 180101(R) (2011).
[24] T. Xu, J. Wang, T. Shimada, and T. Kitamura, J. Phys. Condens. Matter **25**, 415901 (2013).
[25] M. Stengel, Phys. Rev. B **90**, 201112 (2014).
[26] E. K. H. Salje, S. Li, M. Stengel, P. Gumbsch, and X. Ding, Phys. Rev. B **94**, 024114 (2016).
[27] D. W. Cronin, R. G. Petschek, and E. M. Terentjev, J. Chem. Phys. **98**, 9199 (1993).
[28] I. Naumov, A. M. Bratkovsky, and V. Ranjan, Phys. Rev. Lett. **102**, 217601 (2009).
[29] See Supplemental Material at http://link.aps.org/supplemental/10.1103/PhysRevB.96.104102 for the detailed derivations.
[30] A. K. Tagantsev, Phase Trans. **35**, 119 (1991).
[31] N. Marzari and D. Vanderbilt, Phys. Rev. B **56**, 12847 (1997).
[32] V. Sundar and R. E. Newnham, Ferroelectrics **135**, 431 (1992).
[33] R. E. Newnham, V. Sundar, R. Yimnirun, J. Su, and Q. M. Zhang, J. Phys. Chem. B **101**, 10141 (1997).
[34] G. Bester, X. Wu, D. Vanderbilt, and A. Zunger, Phys. Rev. Lett. **96**, 187602 (2006).
[35] H. Grimmer, Acta Crystallogr., Sect. A **63**, 441 (2007).
[36] R. Resta, Rev. Mod. Phys. **66**, 899 (1994).
[37] M. Born and K. Huang, *Dynamical Theory of Crystal Lattices* (Oxford University Press, Oxford, 1954).